Research Article | Vol. 14, No. 12 / 1 Dec 2024 / Optical Materials Express 2874

Optical Materials EXPRESS

Solution-based processing of $Ge_2Sb_2Se_4Te$ optical phase change materials

Daniel Wiedeman,[1,*] Rashi Sharma,[1] Eric Bissell,[2] Parag Banerjee,[2] Casey Schwarz,[3] Brian Mills,[4,5] Juejun Hu,[4] Dennis Callahan,[6] and Kathleen A. Richardson[2,7]

[1]*Chemistry Department, University of Central Florida, 4000 Central Florida Blvd, Orlando, FL 32816, USA*
[2]*Materials Science and Engineering Department, University of Central Florida, 4000 Central Florida Blvd, Orlando, FL 32816, USA*
[3]*Physics and Astronomy Department, Ursinus College, Collegeville, PA 19426, USA*
[4]*Materials Science and Engineering Department, Massachusetts Institute of Technology, Cambridge, MA 02139, USA*
[5]*Draper Scholar Program, The Charles Stark Draper Laboratory, Inc., 555 Technology Square, Cambridge, MA 02139, USA*
[6]*The Charles Stark Draper Laboratory, Inc., 555 Technology Square, Cambridge, MA 02139, USA*
[7]*College of Optics and Photonics, University of Central Florida, 4000 Central Florida Blvd, Orlando, FL 32816, USA*
[*]*daniel.wiedeman@ucf.edu*

Abstract: Phase change materials (PCMs) are important building blocks in solid-state memory and photonic devices. Solution-based processing promises large-area, cost-effective, conformal coating of optical PCMs (O-PCMs) for photonic applications. In this work, a solution processing route was developed for $Ge_2Sb_2Se_4Te_1$ (GSST), a target PCM of interest due to its large optical contrast, broadband transparency, and improved glass-forming capability. An alkahest solvent mixture of ethanedithiol and ethylenediamine was used as a solvent system to fabricate solution-derived GSST thin films and films from these solutions were prepared and characterized using SEM, XRD, and Raman spectroscopy.

1. Introduction

Phase change materials (PCMs) are a group of materials that can be switched between an amorphous and crystalline state [1]. This switching brings about a change in the electric and optical properties of the material making them valuable as components in non-volatile resistive and optical memories [2–4].

One of the most well-known and commercially deployed PCMs today is $Ge_2Sb_2Te_5$ (GST). Developed initially for read-write reversible storage applications where rapid switching speeds were required (300 ns), GST is known for its high refractive index contrast between amorphous and crystalline forms ($\Delta n = 2.2$ at $\lambda = 1.55$ µm [5]) as well as high endurance (10^6 - 10^8 cycles) GST suffers from a major drawback of large optical losses [2,6] in photonic device-relevant applications. These drawbacks limit its use in photonic systems where low loss in both crystalline and amorphous states is required.

Recent advances in PCMs designed for photonic applications include As_2S_3 [7,8], As_2Se_3 [9,10], Sb_2S_3 [11,12], Sb_2Se_3 [12], In_3SbTe_2 [13], and $Ge_2Sb_2Se_4Te$ (GSST) [14,15]. GSST was first proposed and tested in 2017 [15]. It exhibits a high refractive index contrast ($\Delta n = 2.0$), broadband transparency, and an improved glass formability as compared to GST [14]. This makes GSST a unique candidate for metamaterials, integrated photonics, and telecommunications [16,17].

#542387 https://doi.org/10.1364/OME.542387
Journal © 2024 Received 16 Sep 2024; revised 25 Oct 2024; accepted 29 Oct 2024; published 11 Nov 2024

Optical Materials EXPRESS

Thin film deposition of PCMs via sputtering [18,19], pulse laser deposition [18], thermal evaporation (TE) [20], as well as via atomic layer deposition, has been previously reported [21–23]. These techniques offer great control over thickness, uniformity, and elemental composition control of the deposited films, but require significant capital investment and may not be suitable for producing high throughput film deposition on non-planer surfaces. Solution derived (SD) film processing, using techniques such as spin coating [24], dip coating [25], and drop casting [26], offer an opportunity for cost-effective, large area, scalable alternatives to traditionally used thin film deposition techniques.

Solution-based processing strategies for chalcogenides have been studied in the past, yielding numerous solvents, solution chemistries and deposition techniques with varying levels of success in producing high optical quality films. Spin coating has been commonly employed as it is capable of readily producing homogenous thin films with varying thicknesses [24]. Dip coating is a simple and low-cost technique that allows good control and spatial uniformity over a macroscopic film area while obtaining a high uniformity of composition and low roughness, but control over film thickness is limited [25]. Drop casting is as simple as dip coating, both producing less waste solution than spin coating, yet it zallows for more precise, small-area solution deposition [24–26]. Such a method is attractive especially for O-PCMs deposited onto (for example) micro-heater plates where 'pixelated' structures are employed to provide the stimulus for phase change. Of the solvents that have been tested for SD work, hydrazine is among the most promising solvents, as most PCM ingredients exhibit some solubility in it [27,28]. The main issue with hydrazine is its high toxicity and explosive nature, making it not a practical option. Other less hazardous solvents have since been investigated with varying success such as primary amines. Propylamine and n-butylamine are notable solvents for sulfides, while ethylenediamine is more effective at dissolving selenides [7–10,29–34]. The addition of a thiol containing compound, or ethanedithiol, to ethylenediamine has proven useful for increasing solvent power and allowing for telluride solubility as well as sulfides and selenides [35,36].In this work, we report solution chemistry development of GSST using a mixture of ethanedithiol and ethylenediamine for dissolution as it has been shown to be an effective solvent for telluride alloys [35], followed by thin film deposition via drop casting. In our effort, GSST has been dissolved in the solvent mixture and referred to as an "ink", whereas when deposited on a substrate and solvent is removed, it is referred to as "solution derived (SD) film". Dynamic light scattering (DLS) was used to analyze the average particle size of GSST (capable of measuring molecular/particulate clusters of size ~1-10000 nm) when present in the solution. A narrow particle size distribution in the solution is desired, as it allows realization of low-roughness, pinhole-free SD films [37], void of a resulting morphology that creates scattering 'islands'.

In addition to the DLS analysis of GSST solutions, the resulting post-processed SD film's structural, compositional, and morphological properties were studied via scanning electron microscopy (SEM), white light interferometry (WLI), X-ray diffraction (XRD), and Raman spectroscopy (Raman) to assess and quantify morphology, film thickness, surface roughness, crystallinity, and structure, respectively. This work demonstrates a systematic advancement in the fabrication processing and characterization of SD films for photonics applications.

2. Materials and methods

2.1. Bulk alloy preparation of $Ge_2Sb_2Se_4Te_1$

Preparation of GSST bulk alloy was carried out via an alloy-specific melt-and-quench technique [2]. Elements were batched from high purity Germanium (Ge, Alfa Aesar, 99.999% pure, CAS: 7440-56-4), Antimony (Sb, Alfa Aesar, 99.9999% pure, CAS: 7440-36-0), Selenium (Se, American Elements, 99.999% pure, CAS: 7782-49-2), and Tellurium (Te, Alfa Aesar, 99.999+% pure, CAS: 13494-80-9). Batching was done in a glove box (MBraun, LABmaster 130) under N_2 atmosphere ($H_2O < 0.1$ ppm, $O_2 < 0.1$ ppm). The materials were added to a fused silica ampoule

Optical Materials EXPRESS

before sealing under vacuum (10^{-2} torr) with a hydrogen/oxygen torch. The sealed ampoule was then placed in a rocking furnace and heated to 850 °C at 2 °C/min. The furnace was dwelled for 12 hours before quenching at 750 °C in air. The ampoule was left to cool down gradually in ambient temperature. The alloy was then ball milled for 2 hours before sieving to 32-35 µm (450 mesh) using an ultrasonic sieve shaker (MTI Corporation, Compact Ultrasonic Sieving System, MSK-SYU-3) in a glove box. This target particle size was chosen to ensure uniform dissolution of the alloy without aggregation.

2.2. Solvent evaporation

A 1:10 ethanedithiol (Edtsh) to ethylenediamine (EDA) solvent mixture was used in prior work, and it was also shown to be relatively stable over long periods of time [38]. The most stable solution with the highest ratio of Edtsh is desirable to maximize Te dissolution while retaining most of the serviceable lifespan of the solution. While Sb has been shown to be practically insoluble in this solution mixture by itself, it readily reacts with dissolved Se [36]. With Se showing markedly higher solubility than Te, 38 to 9.3 wt% [36], respectively, higher concentrations of Edtsh are better to ensure complete dissolution of the Te component at higher wt%. Incomplete dissolution would affect the desired stoichiometry of the resulting solution prior to deposition, and thus the film. With a higher Edtsh ratio, the solution mixture can be less stable leaving residual salt crystals of solute upon mixing at room temperature. Thus, mild heating (50 °C) and stirring were necessary to dissolve initial salt formation. Once the salt was dissolved the solution remained stable over a long period of time (>2 weeks) given that it is stored under inert gas (N_2).

Preferential solvent evaporation and determination of an appropriate baking protocol for complete removal of solvent with acceptable film quality has been assessed and published in our prior work [38]. Preferential evaporation in our solvent mixture (Edtsh:EDA) was found to favor Edtsh, i.e., the Edtsh in the 1:10 Edtsh:EDA solution evaporates faster than EDA contrary to its lower boiling point (Edtsh 146 °C vs. EDA 116 °C) due to the difference in quantity between the two solvents in solution, 1:10 Edtsh:EDA. The complete removal of solvent was confirmed with energy-dispersive X-ray spectroscopy (EDS) at temperatures of at least 210 °C with some carbon residue (Fig. 1).

2.3. Film production and material characterization

The GSST as-deposited SD films were annealed to drive off solvent without leading to film crazing (cracking) by gradually heating the film at 2 °C/min up to 350 °C for 20 minutes before cooling down slowly. Stable inks must maintain all film constituents in solution, with minimal preferential precipitation which can result in incorrect crystallization stoichiometry upon phase change. SD films were drop-casted by hand via a micro pipette onto the center of TiO_2 coated silicon (Si) substrates (~7 mm x 7 mm). These substrates were on a leveled refractory plate which was slid into the interior of a box furnace within a glove box (MBraun) under N_2 atmosphere (O_2 and H_2O < 0.1 ppm). The TiO_2 coating was used to improve wetting of the solution to realize films with more uniform thicknesses. The heating protocol was determined by monitoring the evaporation of solvent's characteristic peaks using a ThermoFisher Nicolet IS5 FTIR spectrometer. The complete evaporation of the solvent was confirmed via EDS (Fig. 1).

This heating protocol was then used on subsequent films deposited on TiO_2 coated Si substrates. TE GSST films as received from MIT were evaporated using a PVD Products Inc. thermal evaporator. Bulk GSST synthesized using a melt-quench process is crushed and the powder is used as the evaporation source. Deposition is done at a pressure of 1e-5 Torr and substrate temperatures are kept below 40 °C. As deposited films were annealed at 350 °C for 20 mins at a 2 °C/min ramp in inert atmosphere for comparison to the solution deposited films.

Optical Materials EXPRESS

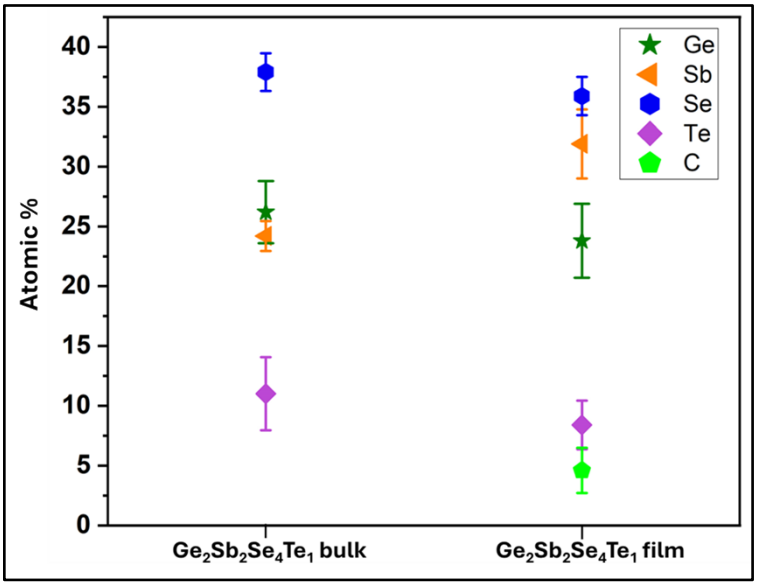

Fig. 1. Atomic percentages within GSST bulk and SD film post.

XRD (PANalytical Empyrean 3 (Cu Kα radiation, λ=1.540598 Å) grazing index XRD with in situ stage heating was used to analyze the crystallization peaks in the films. SEM (Zeiss Ultra 55 FEG) was used to study film morphology. DLS (Malvern Zetasizer Nano-ZS ZEN 3600) was used to characterize the average size dispersion of GSST particles in solution. WLI (Zygo NewView 8000) was used to determine film thickness and surface roughness. Raman (Horiba LabRAM HR Evolution Nano, λ=785 nm (103 mW) at 1%) was conducted to confirm the structural state of films by comparison of SD films to TE films.

3. Results and discussion

3.1. Solution work

As noted, annealing of the as-deposited solution on substrates allows for solvent removal. This process must be slow enough to avoid cracking or pinholes that results from rapid solvent evaporation, to ensure that resulting films have good thickness and morphology uniformity. DLS was performed in ambient air on 1:10 Edsth:EDA solution loaded with 0.1 wt% GSST at both room temperature and at 50 °C. The room temperature spectrum shows an average particle size of 915 ± 184 nm whereas measurement at 50 °C shows an average particle size of 45 ± 13 nm.

The room temperature solution had 20 times larger particle diameters then the solvent at 50 °C, and we attribute this difference in particle size to either incomplete dissolution of GSST, or partial crystallization of salt in the solvent mixture. The mixture of the two solvents (Edtsh, EDA) forms a salt, with chemical formula $(EDAH^{+})_2(Edts^{2-})(EDA)$ [37] that is easily soluble with mild heating (50 °C). This salt formation is only exacerbated by the presence of water and/or O_2.

3.2. Film morphology, structure, and surface characteristics

The target metric in creating PCM films of good optical quality for this study is to achieve a smooth, uniform thickness, pin-hole free film. The loading level of the inks, heating protocol, and volume of the drop-casted ink were tailored to give the best quality film. In Fig. 2, three concentrations of solutions were used while maintaining all other conditions (substrate, area,

Optical Materials EXPRESS

volume of ink, etc.) to determine the optimal concentration of ink for a film. A loading level of 1.25 wt% GSST alloy in solution yielded films of rather poor quality, with an RMS of ~1.673 ± 0.001 μm and grain size of roughly 2 μm, due to an excess of GSST (Fig. 2(a), (b), and (c)). Lowering the loading level of GSST solute to 1.0 wt% while maintaining ink volumes (75 μL) yielded better quality film with reduced grain formation. Here we define 'grains' as macroscopic 'islands' of post-annealed alloy that result from either poor wetting, or compositional variation in the solution that leads to micro-variation in coating uniformity. In some cases, they are clearly spherical in shape (Fig. 2(a)). As shown, the resulting film had a rough surface with an RMS of ~1.936 ± 0.001 μm and pinholes (Fig. 2(d), (e), and (f)). Drop-casting of 0.1 wt% GSST ink solution resulted in a film that was much smoother with an RMS of 0.315 ± 0.001 μm (Fig. 2(i)). The prior two films experienced loss due to scattering when conducting WLI, the black splotches in the WLI images, hence the roughness measurements cannot be accurate. The decrease in scattering with lower weight percentages is then evidence of improving surface roughness. The grain size continued to decrease, along with the coverage of the substrate (Fig. 2(g) and (h)). The platelet particles that make up the grainy structure ranged from 1 μm to 0.1 μm, remaining consistent in size and shape throughout the films (Fig. 2((b), (e), and (h)). Throughout the SEM images, the morphology of the films remained grainy, included holes when sufficient material was present, and was non-uniform. This indicates concentration of the ink does not affect the particle size, but it does determine the coverage and 'grain' growth in the films as lower concentrations at 0.1 wt% do not fully cover the substrate and the 'grains' do not appear in films made from the inks of lower concentration than that of the 1.25 wt%. The appearance of these grains in higher concentrations is concerning, though it is primarily due to the amount of materials present when annealing. We propose that, with the surface completely covered, the excess particulates have one less medium to deposit on. This promotes the growth of these large grains, or agglomerates.

Looking back to the DLS measurements, the average particle size in the ink was 915 ± 184 nm at room temperature and 45 ± 13 nm at 50 °C. The room temperature particle size is clearly representative of the platelet sizes in the SEM analysis (Fig. 2(b), (e), and (h)). All work pertaining to these 3 films was done under a N_2 environment, removing the possibility that salt formation was significantly impacting particle size during DLS measurements. This particle diameter in solution at the time of drop casting indicates GSST particle size was not sufficiently minimized at room temperature.

Prior work shows complete removal of solvent via EDS when the film was heated up to 350 °C at 2 °C/min with a dwell time of 20 min before gradually cooling to room temperature [38]. The thickness of the of the 1.0 wt% film as measured via SEM by taking a cross section is roughly 2 μm in thickness (Fig. 3). The film is relatively uniform throughout the center and raised along the edges due to drop casting the SD film [39].

3.3. Film structure/phase formation

As the film coverage in the 0.1 wt% GSST film (Fig. 2(g)) was insufficient for XRD analysis due to low signal to noise ratio, the 1.0 wt% GSST film (Fig. 2(d)) was used for this analysis. The crystallinity of a GSST drop-casted film was compared to a TE GSST film post annealing at 350 °C for 20 minutes via XRD. Measurements of both the SD and TE films were taken at room temperature, 300 °C, and after the previously thermal cycled film, returned to room temperature (using an in-situ hot stage under flowing Argon atmosphere) to explore the crystallization peak shifts in the films post heating. The XRD analysis of the TE GSST film revealed a single phase of GSST [14], characterized by peaks at 2θ values of 13.5°, 16°, 20.1°, 29.9°, 32.3°, 38.7°, 40.9°, 44.6°, and 54.7°. These peaks are attributed to GeTe (ICDD no. 98-005-6038) and Sb_2Se_3 (ICDD no. 98-008-5676). Additionally, the two prominent peaks at 2θ = 56.5° and 59.7° correspond to Si (ICDD# 00-047-1186). In contrast, the SD films, illustrated in Fig. 4(b), displayed key peaks at 2θ = 18.0°, 29.4°, 39.8°, 44.2°, and 54.0°, which were closely aligned with the TE film peaks,

Optical Materials EXPRESS

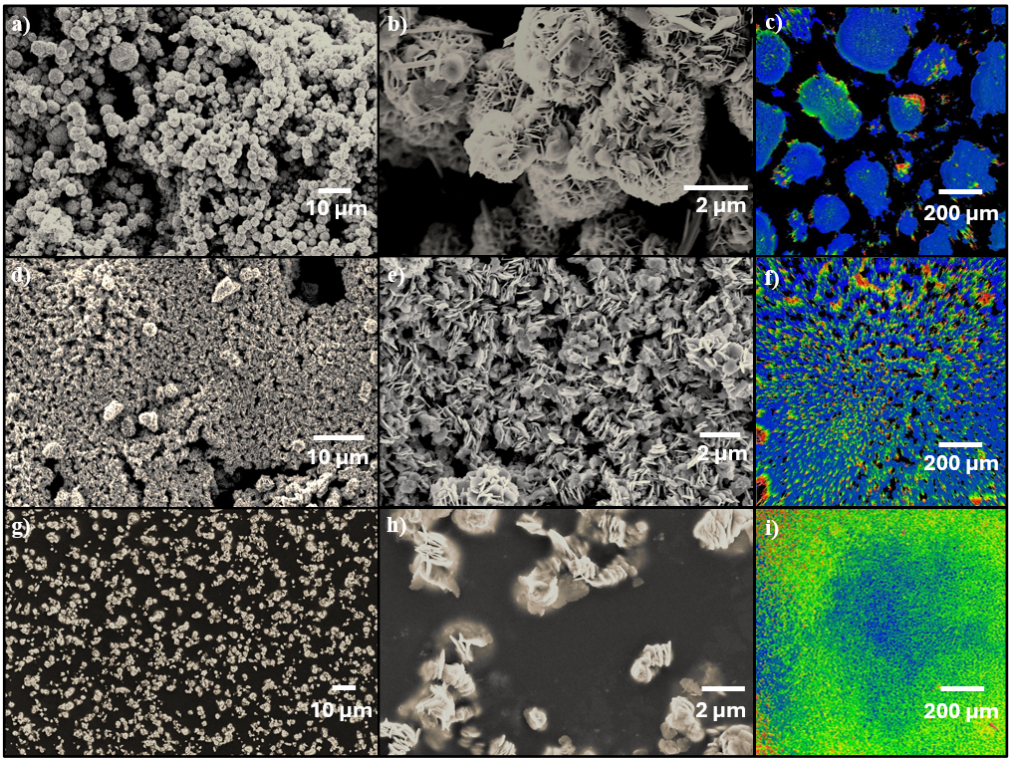

Fig. 2. SEM image of a) 1.25 wt% film (scale bar 10 µm), b) high magnification SEM image of 1.25 wt% film (scale bar 2 µm), c) WLI image of 1.25 wt% film, 75 µL of 1:10 Edtsh:EDA (scale bar 200 µm), SEM image of d) 1.0 wt% film (scale bar 10 µm), e) high magnification SEM image of 1.0 wt% film (scale bar 2 µm), f) WLI image of 1.0 wt% film, 75 µL of 1:10 Edtsh:EDA (scale bar 200 µm), SEM image of g) 0.1 wt% film (scale bar 10 µm), h) high magnification of 0.1 wt% film (scale bar 2 µm), i) WLI image of 0.1 wt% film 75 µL of 1:10 Edtsh:EDA (scale bar 200 µm).

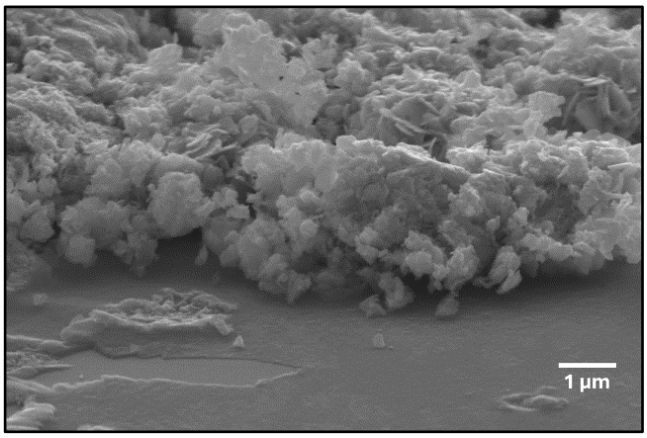

Fig. 3. SEM cross section of 1.0 wt% GSST film.

Optical Materials EXPRESS

though with shifts of less than ~ 1°. This shift can be ascribed to variations in the film deposition techniques. This shows that, while the films do not have completely identical crystalline phases due to their method of deposition, many of the defining crystalline peaks are still evident in the SD film. Both films showed an increase in intensity of all peaks during heating at 300°C along with a slight shift to the left, likely due to the expansion of the material lattice with thermal annealing. Despite this, no new peaks appeared during heating and the peak intensities dropped back to their original strengths after returning to room temperature. The combination of similar prominent peaks with identical stability with heating for both the SD and TE films indicated that the SD methodology, with further improvement on film quality, may serve as a sufficient alternative for producing analogous GSST films to that of TE.

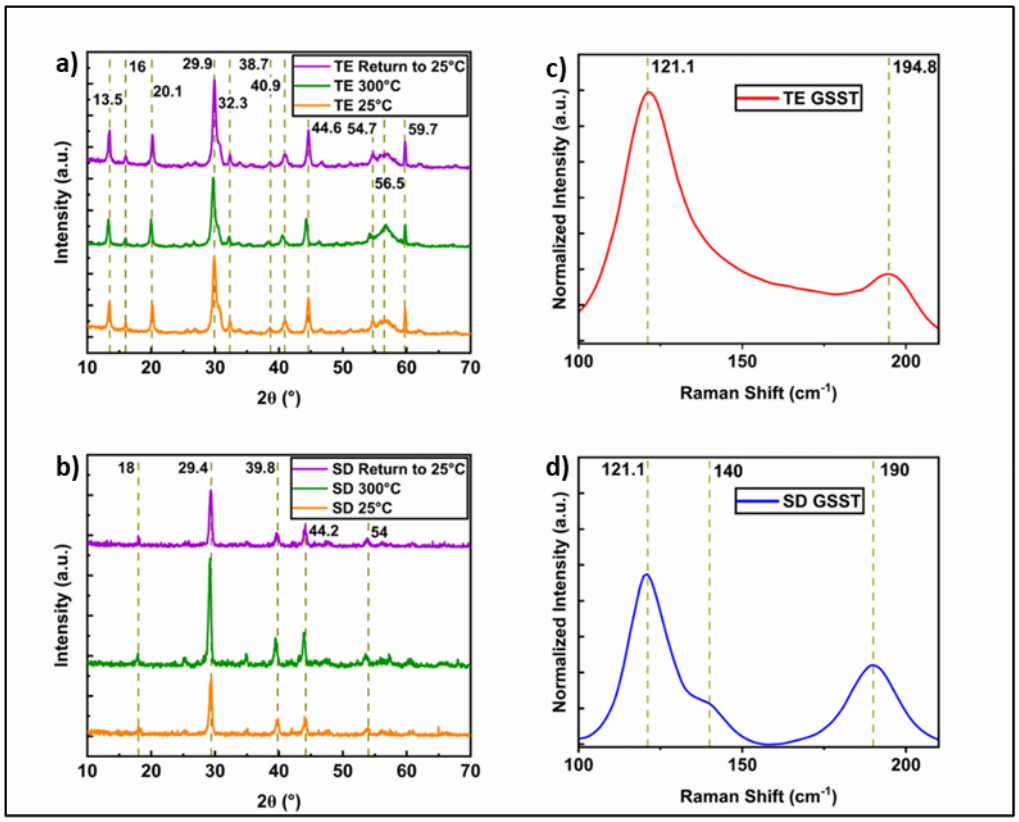

Fig. 4. XRD of (a) TE GSST and (b) drop cast 1.0 wt% GSST films at varying temperatures. Baseline corrected Raman spectrum of annealed (c) TE film and (d) SD 1.0 wt% drop cast films.

The Raman scattering data of the crystalline TE and the SD GSST in Fig. 4(c) and (d), d show bands at 121 cm^{-1} and 194.8 cm^{-1}. These bands were observed in both TE film and SD films, the band at 121.1 cm^{-1} represents the symmetrical stretching mode of corner $GeTe_{4-n}Ge_n$ (n = 0,1,2,3 and 4) [40], whereas the bands at 190 cm^{-1} can be assigned to Sb-Se octahedra as this the location of the most prominent characteristic of Sb_2Se_3 Raman spectrum [41]**.** The shoulder at 140 cm^{-1} was observed only in the SD film can be attributed to pyramid unit of Sb-Te [42]. These two peaks do not bar the Raman from agreeing with the conclusion taken from the XRD data that the films exhibit comparable lattice expansion and stability with heating while having differing crystalline phases. While thermal evaporation deposits material in a disordered form resulting in an amorphous film, solution derived deposition using inks deposits larger, ordered

Optical Materials EXPRESS

particles ranging from 1 μm to 45 nm. The wide range of particle size may contribute to the variation in the XRD and Raman between the TE and SD films.

4. Conclusions

The aim of this work was to investigate the morphological and compositional properties of novel GSST SD thin films via drop casting for potential incorporation into photonic devices. A direct impact on particle sizes within the prepared inks was observed with the temperature during preparation. The particle size in the inks prepared at a 50 °C was found to lower from 915 ± 184 nm at room temperature to 45 ± 13 nm at 50 °C using DLS. The large average particles from room temperature DLS paired with SEM of the drop cast films confirmed the need for smaller particle size in the solution.

A comparison of the TE and SD drop cast films via XRD and Raman spectroscopy explained the observed crystalline phases between the two films. Raman spectroscopy showed that the as deposited TE film was amorphous while the annealing of both the SD drop cast and TE film at 350 °C resulted in a crystalline film, evident in a large peak at 121.1 cm^{-1} [10], and similar peaks throughout the rest of the spectra, though with differing intensities. This data confirmed that both deposition protocols provide the same base elemental make up between the TE and SD drop cast films. The differences in XRD patterns between the TE and SD films show that the deposition techniques result in a SD film resembling that of the TE with minor crystalline peaks. Both TE and SD films showed little change in XRD patterns when heated to 300 °C, and the increased signal intensity with temperature reversed with a return to room temperature showing their stability, with differing thermal history during deposition, at 300 °C is similar. To the best of our knowledge, this is the first time an attempt has been made to deposit SD GSST films on a Si substrate via drop casting using an alkahest solvent mixture (ethanedithiol and ethylenediamine).

The goal of producing high quality GSST films to be incorporated into a microheater array for in-situ monitoring of solid-state phase changes was not realized in this work; however, it is a step towards understanding the film characteristics resulting from SD drop casting as the film does show promising similarity to the TE film in crystalline stability and Raman excitation. Further investigation may prove fruitful for improving the film quality of SD films by increasing the ink viscosity, heated deposition, and/or the use of a reducing agent as a means to reduce GSST particle size in the ink.

Funding. National Science Foundation (DMR#2225967, DMR#1920050, DMR#2225968).

Acknowledgments. Brian Mills acknowledges support from the Draper Scholar Program.

Disclosures. The Authors declare no conflicts of interest related to this article.

Data Availability. Data underlying the results presented in this paper are not publicly available at this time but may be obtained from the authors upon reasonable request.

References

1. C. Constantin-Popescu, M. Shalaginov, F. Yang, *et al.*, "New phase change materials for active photonics," *Conference on Active Photonic Platforms held Part of SPIE Nanoscience and Engineering Conference*, San Diego, CA, Aug 21-25, **12196**, 1219606 (2022).
2. M. Wuttig and N. Yamada, "Phase-change materials for rewriteable data storage," Nat. Mater. **6**(11), 824–832 (2007).
3. M. Stegmaier, C. Ríos, H. Bhaskaran, *et al.*, "Nonvolatile All-Optical 1×2 Switch for Chipscale Photonic Networks," Adv. Opt. Mater. **5**(1), 1600346 (2017).
4. X. Z. Chen, Y. Xue, Y. B. Sun, *et al.*, "Neuromorphic Photonic Memory Devices Using Ultrafast, Non-Volatile Phase-Change Materials," Adv. Mater. **35**(37), 2203909 (2023).
5. M. Rudé, R. E. Simpson, R. Quidant, *et al.*, "Active Control of Surface Plasmon Waveguides with a Phase Change Material," ACS Photonics **2**(6), 669–674 (2015).
6. E. M. Vinod, K. Ramesh, and K. S. Sangunni, "Structural Transition and Enhanced Phase Transition Properties of Se Doped $Ge_2Sb_2Te_5$ Alloys," Sci. Rep. **5**(1), 8050 (2015).
7. Yi Zou, Hongtao Lin, Okechukwu Ogbuu, *et al.*, "Effect of annealing conditions on the physio-chemical properties of spin-coated As2Se3 chalcogenide glass films," Opt. Mater. Express **2**(12), 1723–1732 (2012).

Optical Materials EXPRESS

8. Sivan Tzadka, Natali Ostrovsky, Esti Toledo, *et al.*, "Surface plasticizing of chalcogenide glasses: a route for direct nanoimprint with multifunctional antireflective and highly hydrophobic structures," Opt. Express **28**(19), 28352–28365 (2020).
9. Shanshan Song, Janesha Dua, and Craig B. Arnold, "Influence of annealing conditions on the optical and structural properties of spin-coated As2S3 chalcogenide glass thin films," Opt. Express **18**(6), 5472–5480 (2010).
10. Candice Tsay, Yunlai Zha, and Craig B. Arnold, "Solution-processed chalcogenide glass for integrated single-mode mid-infrared waveguides," Opt. Express **18**(25), 26744–26753 (2010).
11. W. Dong, H. Liu, J. K. Behera, *et al.*, "Wide Bandgap Phase Change Material Tuned Visible Photonics," Adv. Funct. Mater. **29**(6), 1806181 (2019).
12. M. Delaney, I. Zeimpekis, D. Lawson, *et al.*, "A New Family of Ultralow Loss Reversible Phase-Change Materials for Photonic Integrated Circuits: Sb_2S_3 and Sb_2Se_3," Adv. Funct. Mater. **30**(36), 2002447 (2020).
13. S. K. Pandey and A. Manivannan, "Extremely High Contrast Multi-Level Resistance States of In_3SbTe_2 Device for High Density Non-Volatile Memory Applications," Phys. Status Solidi RRL **11**(9), 1700227 (2017).
14. Y. Zhang, J. B. Chou, J. Li, *et al.*, "Broadband transparent optical phase change materials for high-performance nonvolatile photonics," Nat. Commun. **10**(1), 4279 (2019).
15. Y. F. Zhang, J. Y. Li, J. B. Chou, *et al.*, "Broadband Transparent Optical Phase Change Materials," *Conference on Lasers and Electro-Optics (CLEO)*, San Jose, CA, May 14-19, 2017; (2017).
16. H. Shi, L. Zhang, L. Wang, *et al.*, "Ultra-compact integrated photonic switch using miniature phase change material inserted in a slot waveguide," J. Opt. Soc. Am. B **40**(9), 2365–2371 (2023).
17. F. De Leonardis, R. Soref, V. M. N. Passaro, *et al.*, "Broadband Electro-Optical Crossbar Switches Using Low-Loss $Ge_2Sb_2Se_4Te_1$ Phase Change Material," J. Lightwave Technol. **37**(13), 3183–3191 (2019).
18. B. K. Paul, D. Mondal, D. Bhattacharya, *et al.*, "Processing of thin-film electrode based supercapacitors: Progress during the last decade," Comprehensive Materials Processing, Elsevier **2**, 179–199 (2023).
19. I. D. Simandan, F. Sava, A. T. Buruiana, *et al.*, "Influence of Deposition Method on the Structural and Optical Properties of $Ge_2Sb_2Te_5$," Materials **14**(13), 3663 (2021).
20. L. L. Hou, H. Yu, Q. Y. Yao, *et al.*, "Preparation of Mg_2Ge semiconductor thin films by thermal evaporation," Mater. Res. Express **6**(8), 086459 (2019).
21. S. N. Song, L. L. Shen, Z. T. Song, *et al.*, "Phase change properties of Ti-Sb-Te thin films deposited by thermal atomic layer deposition," *International Workshop on Information Data Storage / 10th International Symposium on Optical Storage* 9818, (2016).
22. V. Venkatasamy, I. Shao, Q. Huang, *et al.*, "ALD approach toward electrodeposition of Sb_2Te_3 for phase-change memory applications," J. Electrochem. Soc. **155**(11), D693–D698 (2008).
23. M. Leskelä, V. Pore, T. Hatanpää, *et al.*, "Atomic Layer Deposition of Materials for Phase-Change Memories," ECS Trans. **25**(4), 399–407 (2009).
24. C. H. Rosmani, S. Abdullah, and M. Rusop, "CdSe Thin Film by Using Spin-Coating," Advanced Materials Engineering and Technology **626**, 401–403 (2012).
25. S. Suriani and M. M. Kamisah, "Electrochromic TiO_2 thin film prepared by dip-coating technique," *Solid State Ionics: Trends in the New Millennium, Proceedings*, 439–444 (2002).
26. P. R. Ghediya, T. K. Chaudhuri, V. Raj, *et al.*, "Electrical Properties of Compact Drop-Casted Cu_2SnS_3 Films," J. Electron. Mater. **49**(11), 6403–6409 (2020).
27. D. B. Mitzi, "Solution Processing of Chalcogenide Semiconductors via Dimensional Reduction," Adv. Mater. **21**(31), 3141–3158 (2009).
28. M. Yuan and D. B. Mitzi, "Solvent properties of hydrazine in the preparation of metal chalcogenide bulk materials and films," Dalton Trans. **31**(31), 6065–6236 (2009).
29. C. Tsay, E. Mujagić, C. K. Madsen, *et al.*, "Mid-infrared characterization of solution-processed As_2S_3 chalcogenide glass waveguides," Opt. Express **18**(15), 15523–15530 (2010).
30. Y. Zha, P. T. Lin, L. Kimerling, *et al.*, "Inverted-Rib Chalcogenide Waveguides by Solution Process," ACS Photonics **1**(3), 153–157 (2014).
31. T. Kohoutek, J. Orava, L. Strizik, *et al.*, "Large-area inverse opal structures in a bulk chalcogenide glass by spin-coating and thin-film transfer," Opt. Mater. **36**(2), 390–395 (2013).
32. S. M. R. Ullah, A.-A. A. Simon, and M. Mitkova, "Studies and analysis of Ge_xSe_{100-x} Based Spin Coated Chalcogenide Thin Films," Microsc. Microanal. **25**(S2), 2608–2609 (2019).
33. S. Slang, K. Palka, L. Loghina, *et al.*, "Mechanism of the dissolution of As–S chalcogenide glass in n-butylamine and its influence on the structure of spin coated layers," J. Non. Cryst. Solids **426**, 125–131 (2015).
34. J. Jancalek, S. Slang, M. Kurka, *et al.*, "Preparation of quaternary solution processed chalcogenide thin films using mixtures of separate As40S60 and Ge20Sb5S75 glass solutions," J. Non. Cryst. Solids **564**, 120833 (2021).
35. D. H. Webber and R. L. Brutchey, "Alkahest for V_2VI_3 Chalcogenides: Dissolution of Nine Bulk Semiconductors in a Diamine-Dithiol Solvent Mixture," J. Am. Chem. Soc. **135**(42), 15722–15725 (2013).
36. D. H. Webber, J. J. Buckley, P. D. Antunez, *et al.*, "Facile dissolution of selenium and tellurium in a thiol-amine solvent mixture under ambient conditions," Chem. Sci. **5**(6), 2498–2502 (2014).
37. K. M. Koskela, M. J. Strumolo, and R. L. Brutchey, "Progress of thiol-amine 'alkahest' solutions for thin film deposition," Trends in Chemistry **3**(12), 1061–1073 (2021).

Optical Materials EXPRESS

38. M. Kang, R. Sharma, C. Blanco, *et al.*, "Progress on Solution-Derived Ge-Sb-Se-Te Chalcogenide Films as a Candidate for High Figure-of-Merit Optical Phase Change Materials," Sci. Rep. **14**(1), 18151 (2024).
39. A. K. S. Kumar, Y. F. Zhang, D. L. Li, *et al.*, "A mini-review: How reliable is the drop casting technique?" Electrochem. Commun. **121**, 106867 (2020).
40. A. Ali, S. M. Ansari, B. Ehab, *et al.*, "Effect of vacuum annealing on structural and electrical properties of germanium telluride thin films and Broadband nonvolatile photonic switching based on optical phase change materials: beyond the classical figure-of-merit," Opt. Lett. **43**(1), 94–97 (2018).
41. A. Shongalova, M. R. Correia, B. Vermang, *et al.*, "On the identification of Sb_2Se_3 using Raman scattering," MRS Commun. **8**(3), 865–870 (2018).
42. A. A. Burtsev, N. N. Eliseev, V. A. Mikhalevsky, *et al.*, "Physical properties' temperature dynamics of GeTe, $Ge_2Sb_2Te_5$ and $Ge_2Sb_2Se_4Te_1$ phase change materials," Mater. Sci. Semicond. Process. **150**, 106907 (2022).